Plasma Physics and Controlled Fusion

Favourable effect of methane discharges observed in LHD pellet shots

To cite this article: J Miyazawa *et al* 2002 *Plasma Phys. Control. Fusion* **44** A203

INSTITUTE OF PHYSICS PUBLISHING PLASMA PHYSICS AND CONTROLLED FUSION

Plasma Phys. Control. Fusion **44** (2002) A203–A209 PII: S0741-3335(02)34300-8

Favourable effect of methane discharges observed in LHD pellet shots

J Miyazawa, H Yamada, R Sakamoto, K Tanaka, S Morita, S Sakakibara, M Osakabe, M Goto, O Kaneko, K Kawahata, A Komori, S Murakami, S Muto, K Narihara, N Ohyabu, B J Peterson, A Sagara, T Tokuzawa, K Y Watanabe, Yuhong Xu, K Yamazaki and LHD Experimental Group

National Institute for Fusion Science, Toki, Gifu 509-5292, Japan

E-mail: miyazawa@LHD.nifs.ac.jp

Received 5 September 2001
Published 25 April 2002
Online at stacks.iop.org/PPCF/44/A203

Abstract
The improvement in the particle confinement of pellet shots on the Large Helical Device (LHD) was found after methane (CH_4) mixed hydrogen gas-puff discharges. Only four discharges introducing $\sim$20 Pa m^3 of CH_4 caused the reduction in the radiation loss and the level of metal impurities, together with the enhanced recycling, which is expected as the real time carbonization effect. The decay rate of the electron density was mitigated in the pellet shot after CH_4 discharges. Transport analysis shows 60% reduction in the particle transport coefficient at half the averaged minor radius.

1. Introduction

Since October 1999, the Large Helical Device (LHD) [1] has been equipped with carbon divertor tiles that cover the full trace of the divertor legs [2]. The influx of metal impurities has been significantly reduced, while the emission from carbon ions has been increased [3]. However, these influences of carbon divertor tiles were conspicuous only just after the installation. On the other hand, the confinement property of LHD plasmas shows the gyro-Bohm nature [4], where the energy confinement time inversely depends on the ion gyro-radius, and a recent study has pointed out the importance of the effective charge Z_{eff} that affects the averaged ion gyro-radius [5]. Hence, impurity control is the key to understanding the confinement nature of LHD plasmas.

In tokamaks, a number of impurity-induced confinement improvement has been reported, i.e. Z-mode in ISX-B [6], RI-mode in TEXTOR-94 [7], TFTR [8], and DIII-D [9]. In these experiments, noble gases were injected for impurity species. Also in LHD, neon gas-puff has been used for the charge-exchange emission measurement [10]. However, its applicable regime was limited to electron densities less than 1×10^{19} m^{-3}. Neon injection in the high-density regime usually caused the radiation collapse of LHD plasmas heated by up to 4.5 MW of neutral beam injection (NBI). Methane (CH_4) as an impurity for injection has less risk of radiation collapse compared with neon, since the cooling rate of carbon is smaller than that of neon in the high-temperature regime [11]. During CH_4 discharges, the carbon impurities are piled on the wall, and the aftereffect of this carbon accumulation can last. This is called the real time carbonization (RTC) and can work to reduce metal impurities. This technique was applied as the real time bolonization (RTB) in CHS, where a small amount of decaborane puffed into NBI-heated plasmas reduced the metal and oxygen impurities [12].

The CH_4 mixed hydrogen gas-puff experiment was carried out on LHD, to test the possibility of impurity control and the feasibility of RTC. Although the CH_4 mixed discharges itself did not show clear differences compared with the hydrogen gas-puff shots, only four discharges introducing $\sim$20 Pa m^3 of CH_4 (consisting of about 5×10^{21} carbon atoms) caused the reduction of metal impurity emission, together with increased confinement in the shot fuelled by hydrogen ice-pellets [13]. In this paper, the effect of CH_4 discharges on the confinement property is investigated; especially we perform the transport analysis of pellet shots before and after CH_4 discharges.

2. CH_4 gas-puff experiment

Results of experiments to test the feasibility of RTC are demonstrated in figure 1, where the maximum plasma stored energy, $(W_p)_{max}$, the level of C III emission, the radiation loss, P_{rad}, and the ratio of τ_E^{EXP} to τ_E^{ISS95}, $F_{ISS95} (= \tau_E^{EXP}/\tau_E^{ISS95}$; τ_E^{EXP} is the experimental energy confinement time and τ_E^{ISS95} is that expected from the international stellarator scaling 95 (ISS95) [14]), are shown from top to bottom, and the abscissa is the line-averaged electron density, $\bar{n}_e$. These discharges were carried out continuously in a day with the typical experimental parameters fixed; i.e. the magnetic field strength on the magnetic axis, $B_0 \sim 2.85$ T, the major radius of the magnetic axis, $R_{ax} = 3.6$ m, and the averaged minor radius of the plasma, $a \sim 0.6$ m. All of the data points are extracted from NBI-heated discharges of 3.6–4.5 MW total heating power, P_{NB}. Here, P_{NB} is estimated from direct heat-load measurement of NB shine-through power [15], which shows sufficient agreement with the three-dimensional Monte Carlo simulation [16] in the dense plasmas of $\bar{n}_e > 2 \times 10^{19}$ m^{-3}. Typical LHD plasma shows a favourable dependence of $W_p \propto \bar{n}_e^{0.51}$, as predicted by ISS95 scaling [14]. A deterioration of the scaling in the high-density regime ($\bar{n}_e > 5 \times 10^{19}$ m^{-3}) can be seen in figure 1(*a*), where F_{ISS95} also decreases (see figure 1(*d*)). Four successive CH_4 mixed hydrogen gas-puff discharges were carried out, introducing about 20 Pa m^3 of CH_4 in total. Data from two of the four CH_4 discharges are also depicted by open triangles in figure 1, which has slightly improved F_{ISS95} compared with that before the CH_4 discharges. Meanwhile, significant differences are observed between the pellet shots before and after CH_4 discharges, where $(W_p)_{max}$, the emission of C III, and F_{ISS95} systematically increase, and P_{rad} for higher density decreases after CH_4 discharges. The cause of the difference between the pellet and the gas-puff shots is not fully understood at this moment, and hence not discussed in this study. Hereinafter, we focus on the differences in the pellet shots before and after the CH_4 discharges.

3. Comparison of the pellet shots before and after the CH_4 discharges

3.1. Phenomenological differences

Two typical pellet shots before and after CH_4 discharges are compared in figure 2. At the time $t = t_0 = 1.1$ s in both discharges, W_p, $\bar{n}_e$, P_{NB}, and the electron temperature T_e are almost the same. However, the decay time of $\bar{n}_e$ in the pellet shot after CH_4 discharges (#23114) is

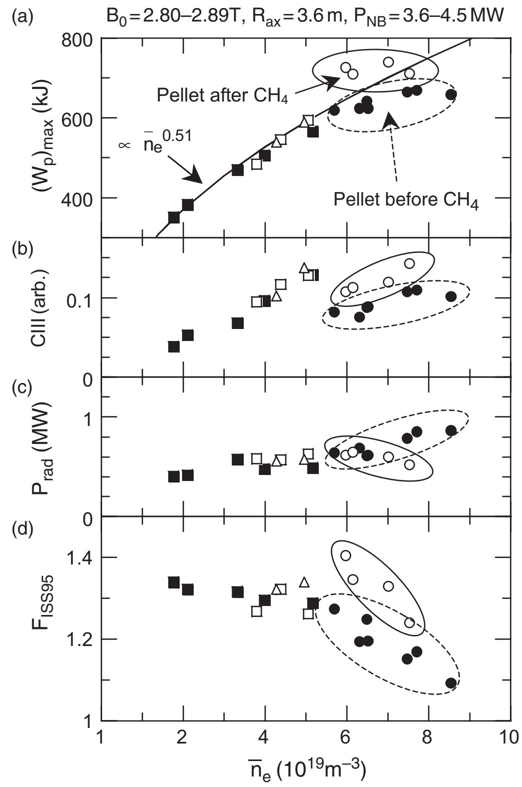

Figure 1. Typical plasma parameters in relation to the line-averaged electron density, $\bar{n}_e$. Here, (*a*) $(W_p)_{max}$, (*b*) the intensity of C III emission, (*c*) P_{rad}, and (*d*) F_{ISS95} are shown from top to bottom. Solid and open circles (squares) denote pellet (gas-puff) shots before and after CH_4 mixed hydrogen gas-puff discharges (open triangles), respectively.

mitigated to about twice that before CH_4 discharges (#23046). This directly results in the larger W_p for $t > t_0$, since the temporal behaviours of T_e are almost the same. Here we compare the time slice of #23046 at $t = t_1 = 1.25$ s and that of #23114 at $t = t_1' = 1.4$ s, to keep $\bar{n}_e$ in both slices the same. In these time slices, the energy confinement time and F_{ISS95} in #23114 are larger than that in #23046, since P_{NB}, dW_p/dt (~ 0), and $\bar{n}_e$ are identical. As shown in figures 2(*b*) and (*c*), the total radiation loss, P_{rad}, and the emission of Fe XVI become smaller after CH_4 discharges. This suggests the reduction of metal impurity, which is expected as the RTC effect. Metal impurity reduction is also seen in the soft x-ray spectra, where the K_α lines of Ti, Cr, and Fe are significantly reduced in #23114.

To see the difference between these two shots more precisely, radial profiles of the electron density, $n_e(\rho)$, the electron temperature, $T_e(\rho)$, and the radiation loss power density, $p_{rad}(\rho)$, are compared in figure 3 ($\rho = r/a$ is the normalized minor radius). The radial profiles at $t = t_0$ and $t = t_1$ of #23046 and those at $t = t_0$ and $t = t_1'$ of #23114 are chosen to compare the change in T_e and p_{rad} profiles, while keeping the similar n_e profile. As seen in figure 3(*a*), n_e profiles of #23114 have humps at the plasma boundary of $\rho > 0.8$, indicating relatively enhanced recycling after CH_4 discharges. There are also other indications of the enhanced recycling in the divertor flux and the neutral pressure, i.e. both of them increased significantly after CH_4 discharges. However, the n_e profiles inside the plasma ($\rho < 0.7$) are almost identical. This

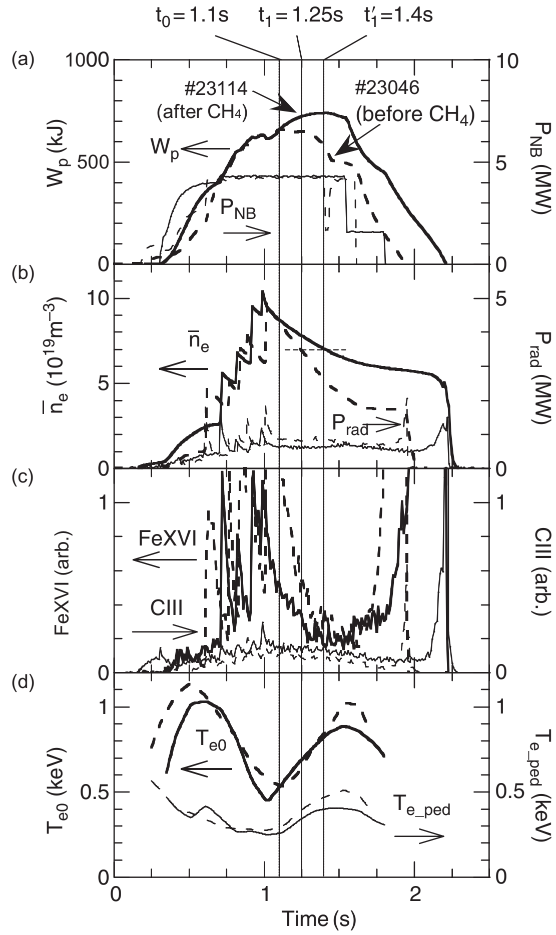

Figure 2. Waveforms of (*a*) W_p and P_{NB}, (*b*) $\bar{n}_e$ and P_{rad}, (*c*) the emission intensities of Fe XVI and C III, and (*d*) the electron temperature at the plasma centre, T_{e0}, and the pedestal ($\rho = 0.9$), $T_{e\text{-ped}}$. Broken and solid lines denote #23046 (before CH_4 discharges) and #23114 (after CH_4 discharges). Times t_1 and t_1' are chosen so that values of $\bar{n}_e$ are the same.

suggests that the particle source from the enhanced recycling is negligible in the core region. As for the T_e profiles (figure 3(*b*)), there is a significant difference between #23046 ($t = t_1$) and #23114 ($t = t_1'$). After CH_4 discharges, the central electron temperature increases up to 120% of that before CH_4 discharges. Metal impurity reduction is recognized again in the p_{rad} profiles shown in figure 3(*c*), where the hump observed at $\rho \sim 0.6$ in #23046 disappears in #23114. Whether the increase in T_e is due to the reduction of p_{rad} is studied in the next subsection.

3.2. Transport analysis

3.2.1. Particle transport. Particle transport analysis is carried out using the n_e profile such as shown in figure 3(*a*). Here, the particle diffusion coefficient, D, and the convection velocity, V, are directly estimated from the temporal behaviour of the n_e profile [17]. The particle balance

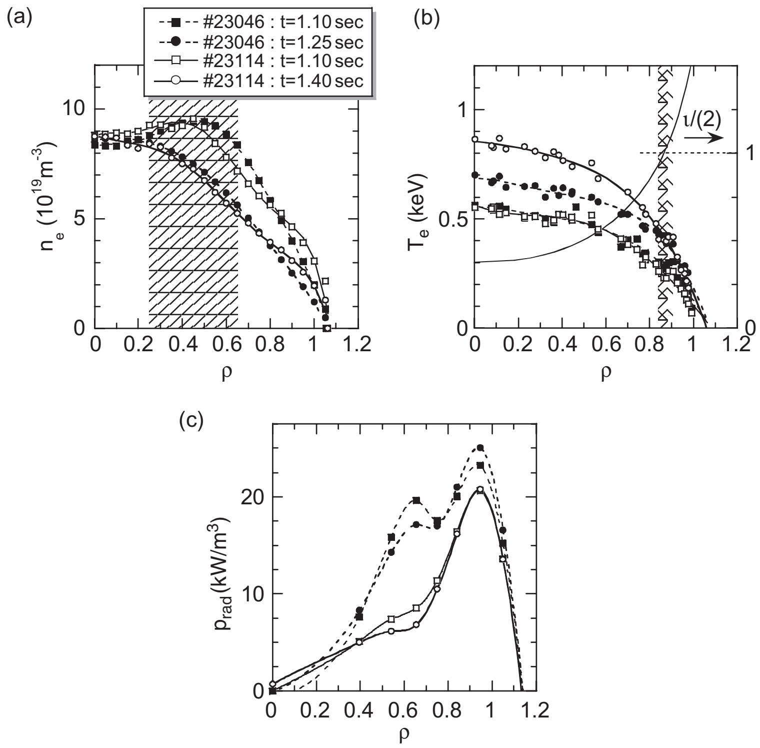

Figure 3. Radial profiles of (a) n_e, (b) T_e and the rotational transform, ι, and (c) p_{rad}. The hatched region in (a) is where the particle transport analysis is carried out, and that in (b) indicates the position of the magnetic island at $\iota \sim 1$.

equation is given as

$$\frac{\partial n_e}{\partial t} = -\nabla \cdot \Gamma + S = -\frac{1}{r}\frac{\partial}{\partial r} r\Gamma + S, \tag{1}$$

where S is the particle source rate and Γ is the particle flux defined by

$$\Gamma = -D\frac{\partial n_e}{\partial r} + V n_e. \tag{2}$$

Integrating equation (1) with r, $\Gamma(r)$ is expressed as

$$\Gamma(r) = \frac{1}{r}\int_0^r r\left(S - \frac{\partial n_e}{\partial t}\right)\mathrm{d}r. \tag{3}$$

It is straightforward from equation (2) that a linear regression $y = Ax + B$ of a scatter plot with $x = (\mathrm{d}n_e/\mathrm{d}r)/n_e$ and $y = \Gamma/n_e$ at fixed position ρ gives $D(\rho)$ as $-A$ and $V(\rho)$ as B. Using this method, the radial profiles of D (figure 4(a)) and V (figure 4(b)) are obtained. The number of time points used for the fitting is 16 (31) for #23046 (#23114). Note that the analysis is carried out in the region of $\rho = 0.25$–0.65 assuming $S = 0$. Since the particle source from the recycling is localized in the plasma edge ($\rho > 0.65$), and the particle source from NBI is less than 10^{19} m^{-3} s^{-1} while the typical order of $-\mathrm{d}\bar{n}_e/\mathrm{d}t$ in this region is around 10^{20} m^{-3} s^{-1}, the assumption of $S = 0$ is acceptable. It can be concluded from figures 4(a) and (b) that the value of D is reduced to 35–45% after CH_4 discharges, while V is almost unchanged and nearly zero in the core region of $\rho < 0.5$.

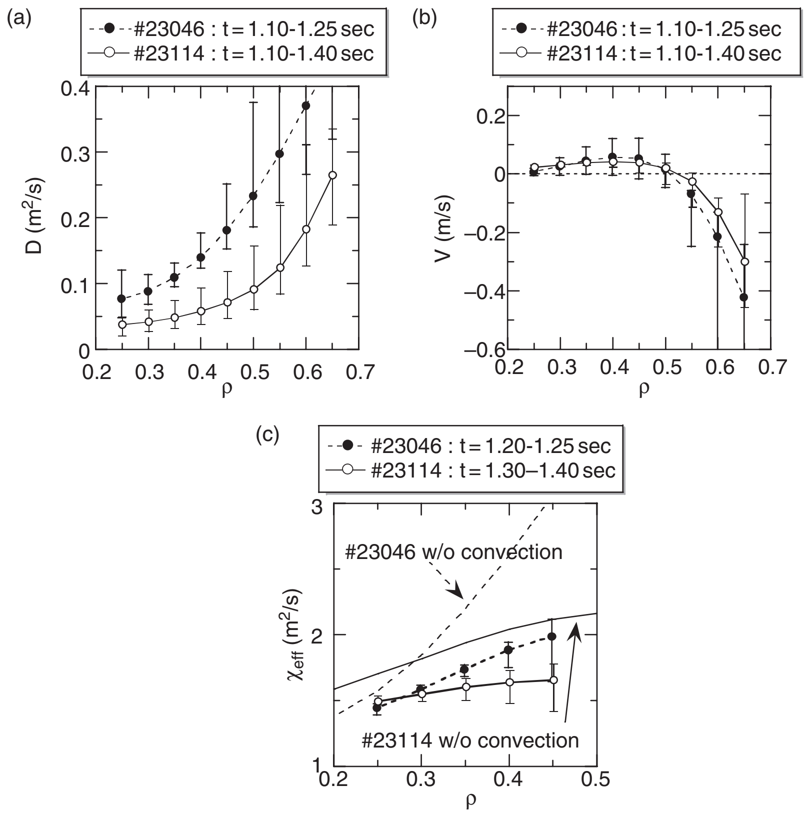

Figure 4. Radial profiles of (*a*) D, (*b*) V, and (*c*) $\chi_{\rm eff}$. Radial profiles of broken and solid lines denote #23046 (before CH_4 discharges) and #23114 (after CH_4 discharges), respectively. The error bars in (*a*) and (*b*) denote the upper and lower limits of estimation resulting from the error in the Abel inversion of the $n_{\rm e}$ profile. The error bars in (*c*) are calculated from that of D. The thin broken (solid) line in (*c*) is the estimation of $\chi_{\rm eff}$ without considering the convection term in #23046 (#23114).

3.2.2. Thermal transport. The effective thermal transport coefficient, $\chi_{\rm eff}$, is directly derived from the energy balance equation:

$$3\frac{\partial\,(nT)}{\partial t} = \frac{1}{r}\frac{\partial}{\partial r}r\left(2n\chi_{\rm eff}\frac{\partial T}{\partial r} - 5T\Gamma\right) - p_{\rm rad} + p_{\rm NB}, \qquad (4)$$

where $p_{\rm rad}$ and $p_{\rm NB}$ are the radiation loss power density and the total heating power density of NBI, respectively. Note that we assumed $n = n_{\rm e} = n_i$, $T = T_{\rm e} = T_{\rm i}$, and $\Gamma = \Gamma_{\rm e} = \Gamma_{\rm i}$. Using profiles at $t = 1.2$–1.25 s of #23046 and that at $t = 1.3$–1.4 s of #23114, $\chi_{\rm eff}$ profiles are estimated and shown in figure 4(*c*). Here the particle flux Γ is calculated using the result obtained in the former subsection, and $p_{\rm NB}$ is calculated by the three-dimensional Monte Carlo simulation [16]. In figure 4(*c*), thin solid and broken lines denote the $\chi_{\rm eff}$ estimated without the convection term of $-5T\Gamma$. Even taking into account the large contribution of the convection term in #23046, the $\chi_{\rm eff}$ is still smaller in #23114. Although the profile of $p_{\rm rad}$ significantly differs in these two shots as seen in figure 3, this is not influential because $p_{\rm NB}$ is about ten times larger than $p_{\rm rad}$. The difference of $\chi_{\rm eff}$ between the two shots mainly comes from the large difference in the $n{\rm d}T/{\rm d}r$ profile.

In conclusion, the effective thermal transport is improved after CH_4 discharges. This improvement is not a direct resultant from the reduction of radiation loss. There will be a hidden mechanism for the improvement, which will be studied in future.

4. Summary and discussion

CH_4 gas-puff experiment has been carried out on LHD. Although the CH_4 discharges itself showed only a slight difference compared with the hydrogen gas-puff shots, a significant improvement was observed in the shots fuelled with hydrogen ice-pellets, following the CH_4 discharges. The intensity of metal impurity emissions in the visible and soft x-ray range, the total radiation loss, and the hump observed in the p_{rad} profile are largely reduced in the pellet shots after CH_4 discharges. These phenomena together with the increased n_{e} at the edge region are that expected as the RTC effect.

In addition, the decreasing rate of n_{e} was mitigated in the pellet shot after CH_4 discharges. The transport analysis has revealed 40% reduction in D at $\rho = 0.5$, and χ_{eff} was also reduced. The improvement in the confinement is not due to the reduction of the radiation loss, but due to the reduction of D and χ_{eff}. The scenario which connects the phenomenological observations of the RTC effect and the improvement in both the particle and the effective thermal transport has not been discussed here. To answer this, more detailed and systematic experiments together with the various measurements on the electrostatic fluctuation and magnetic fluctuation will be necessary.

Acknowledgments

The authors would like to thank all the members of the LHD team, including technicians and graduate students of Nagoya University and the Graduate University of Advanced Studies. It would not have been possible to carry out the LHD experiments without their dedication and effort.

References

[1] Fujiwara M *et al* 1996 *J. Fusion Energy* **15** 7
Motojima O *et al* 1999 *Phys. Plasmas* **6** 1843
[2] Noda N *et al* 2000 *J. Plasma Fusion Res. S.* **3** 180
Noda N *et al* 2001 *Nucl. Fusion* **41** 779
[3] Morita S *et al* 2001 *Phys. Scr.* **T91** 48
[4] Yamada H *et al* 2000 *Phys. Rev. Lett.* **84** 1216
Yamada H *et al* 2001 *Nucl. Fusion* **41** 901
[5] Miyazawa J *et al* 2001 paper presented at the *28th EPS Conf. on Controlled Fusion and Plasma Physics (Madeira)* p 4.043
[6] Lazarus E A *et al* 1984 *J. Nucl. Mater.* **121** 61
[7] Messiaen A M *et al* 1996 *Phys. Rev. Lett.* **77** 2487
[8] Hills K W *et al* 1999 *Phys. Plasmas* **6** 877
[9] McKee G R *et al* 2000 *Phys. Plasmas* **7** 1870
[10] Ida K, Kado S and Liang Y 2000 *Rev. Sci. Instrum.* **71** 2360
Ida K *et al* 2001 *Phys. Rev. Lett.* **86** 5297
[11] Post D E *et al* 1977 *At. Data Nucl. Tables* **20** 397
[12] Sagara A *et al* 1997 *J. Nucl. Mater.* **241–243** 972
[13] Sakamoto R *et al* 2001 *Nucl. Fusion* **41** 381
[14] Stroth U *et al* 1996 *Nucl. Fusion* **36** 1063
[15] Osakabe M *et al* 2001 *Rev. Sci. Instrum.* **72** 590
[16] Murakami S, Nakajima N and Okamoto M 1995 *Trans. Fusion Technol.* **27** 256
[17] Tanaka K *et al* 1999 *Proc. 26th EPS Conf. on Controlled Fusion and Plasma Physics (Maastricht)* ECA vol 23J, p 1329